Available online at www.sciencedirect.com

ScienceDirect

journal homepage: www.elsevier.com/locate/he

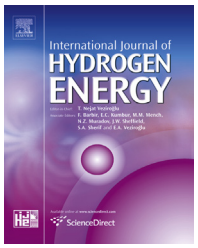

Simulation of thermal stresses for new designs of microtubular Solid Oxide Fuel Cell stack

P. Pianko-Oprych[*], *T. Zinko*, *Z. Jaworski*

West Pomeranian University of Technology, Szczecin, Faculty of Chemical Technology and Engineering, Institute of Chemical Engineering and Environmental Protection Processes, Al. Piastów 42, 71-065 Szczecin, Poland

ARTICLE INFO

Article history:
Received 30 December 2014
Received in revised form
21 May 2015
Accepted 25 May 2015
Available online 14 June 2015

Keywords:
Simulation
Thermal stresses
Microtubular Solid Oxide Fuel Cell stack
Computational fluid dynamics
Computational structural mechanics
Optimization design

ABSTRACT

The aim of this study was to improve design of microtubular Solid Oxide Fuel Cell (mSOFC) stacks. Three-dimensional models were developed in order to investigate the effect of flow channel and fuel cells arrangement on thermal stresses of the mSOFC stacks and their performance. Two geometries of the anode-supported mSOFC stack were considered. The paper presents modifications of fuel cell arrangement in the stacks and analyses for two ways of stack cooling carried out by coupling a Computational Fluid Dynamics (CFD) and Computational Structural Mechanics (CSM). The simulation results indicate that the lowest value of the total displacement of the assembly was noticed for the mSOFC stack design with an external air flow cooling (case H–E). In addition, the smallest axial and total stresses were recognized for the same case H–E due to uniform temperature distribution, which limits strain of the materials and prevents development of excessive thermal stresses in the mSOFC stack components.

Introduction

Microtubular Solid Oxide Fuel Cell stacks (mSOFC) provide the simplest possible method of delivering electric and thermal energy with a high efficiency above 90% [1]. However, use of conventional fuels like hydrogen or LPG causes high operating temperatures of mSOFC stacks in the range of 650–900 °C. High temperature may cause damage of a fuel cell stack due to stress concentration problems. In addition, performance instability of a SOFC stack can result from mechanical instability of its structure subjected to moderate stress. Stress applied to ceramic components can arise from residual stresses due to manufacturing, differential thermal expansion coefficient (CTE) of cell layers, spatial or temporal temperature or oxygen gradients as well as external mechanical loading [2].

In particular, thermal stresses, which are the function of the applied material CTEs have direct impact on the performance of a system operating at high temperatures typical for SOFCs working conditions. Therefore, a key role in the fuel cell designing and its improvement is played by thermal management. Only a few numerical investigations were conducted to improve thermal behaviour of the SOFC stacks by introducing a second air stream for the purpose of better cooling [3] or by changing the flow geometry to reduce heterogeneity in reactant distribution over the active area [4].

* *Corresponding author*. Tel.: +48 91 449 47 31.
E-mail address: paulina.pianko@zut.edu.pl (P. Pianko-Oprych).
http://dx.doi.org/10.1016/j.ijhydene.2015.05.164

Vijay et al. [3] proposed a modification of interconnect design, which includes several holes that allow to transfer material from the high pressure secondary channel to the low pressure primary channel. Moreover, including the secondary air flow in the counter current direction to the fuel flow resulted in lesser temperature gradients across a fuel cell and minimizing thermal stresses in the cell [3]. Grondin et al. [5] developed a 3D model to investigate the effect of interconnect design on electrical performance and degradation processes. Cathode degradation was supposed to be due to temperature gradient non-uniformities and a strong impact of cathode/interconnect contact on thermal and electrical behaviour was shown. These studies [3–5] demonstrated that the fuel cell physical design played an essential role in determining thermal stress distributions.

The efforts to increase the reliability of SOFC components were put during a feasibility study considering the geometrical effect of the wire mesh structure on the thermomechanical behaviour of a 36 layer planar SOFC stack [6]. Nonlinear elastoplastic behaviour of an interconnector plate as well as the poor flow pattern that resulted in thermomechanical differences within the stack were considered. The results showed that the thermomechanically induced stress within the stack sealants was driven mostly due to the elastoplastic behaviour of steel components as the yielding steel caused higher strain, reducing the stress within the steel. This in turn made the sealant subjected to high tensile stress and as a result the sealant was susceptible to failure. Due to the fact that hermetic sealing of planar SOFC components is a critical issue it was a subject of further Peksen's et al. [7] considerations. The non-linear elastoplastic behaviour of the metal stack components as a function of temperature during thermal cycling was studied to determine the mechanisms that trigger the thermomechanically induced stress when the heating up, operation and shutdown stages were considered. It was noted that during the early stage of the heating up thermomechanically induced stress was higher by a factor two in comparison to the time the assembly reached a minimum temperature of 723 °C. The regions susceptible to stress at the fillet regions and ribs were reduced over time as the temperature was risen and retained at lower values. The conclusion was that the assembly was subjected to the highest thermomechanical load an initial stage of the heating-up process and needed to be carefully controlled [7]. During the operation stage it was found that sealant materials were influenced mainly due to the elastic and plastic behaviour of the metal components. Depending on the softness or hardness of the sealant, the sealants resisted or allowed to move and influenced the amount of the resultant stress. Within the early stages of the shutdown stage the linear thermal expansion coefficient decreased by 8%, the temperature difference by 416 °C for time period of 7500 s and was reduced to 247 °C at the time instant of 22,500 s. That means that the local temperature had the greatest influence to the thermal strain and the thermal strain was the dominating thermomechanical stress [7]. Thus, it was shown that the model enables identification of critical locations of the fuel cell assembly and provides detailed information about the strain and stress within the whole SOFC stack over time.

A relationship between mechanical and electrochemical degradation aspects, which affect the SOFC stack durability during long-term operation and thermal cycling was investigated also by Nakajo et al. [8]. Quantitative factors based on the probability of failure were proposed for detailed study. It was noticed that even a subtle changes in the mechanical properties of the materials or an interaction between the stack components may result in their failure. Modification of the temperature profile caused by electrochemical degradation during operation at constant system power modified the probability of failure of the cell, which depend upon the operating conditions. Therefore, the level of coupling between thermos-electrochemical and mechanical aspects, restricted in the study [8] to discrete importing of the temperature profile have to be enriched to include the whole complexity of the real situation.

In addition, the need of a better understanding of the cell's performance under stack operating conditions was recognized by Boigues-Munoz et al. [9]. A good stack compactness was achieved by employing two different tubular cell configurations enabling a more effective interconnectivity with minimum disruption of the air stream. It was noticed that a tight coiling around the anode avoids an undesirable exposure to the air stream, which can potentially lead to re-oxidation of the nickel matrix and also cause mechanical stress.

Moreover, recent progress in experimental capabilities represented by the non-destructive X-ray holotomography or the combination of sample sectioning by Focused Ion Beam with imaging by Scanning Electron Microscopy techniques has enabled to conduct three-dimensional numerical reconstruction of the SOFC electrode microstructures [10]. Information on the 3D reconstructed SOFC electrodes made it possible to determine the relation between microstructural parameters, processes and macroscopic properties such as thermos–mechanical properties. Delette et al. [10] found that the effective elastic parameters were influenced by morphological parameters such as porosity or formation factor that can be also related to the manufacturing process. However, these morphological parameters had negligible effect on the effective thermal expansion.

It has been observed that in most of the reported modelling work, thermal stress analysis is crucial in optimization of stack geometry and system performance. However, none of the considered studies provided a detailed comparison of the temperature gradients and thermal stresses for 3D geometry of an anode-supported microtubular Solid Oxide Fuel Cell stack containing the same number of fuel cells, but different flow channel and fuel cells arrangement. Therefore, the main aim of this work is to study thermal stresses in three different configurations of the mSOFC stack, compare of the temperature/thermal stress fields and indicate an optimal configuration of the mSOFC stack design that reduces temperature gradients and consequently the stack thermal stresses.

Numerical methodology

The numerical methodology based on a similar approach to that used by Wei et al. [11] and Peksen [12]. The predictions of thermal stresses in microtubular Solid Oxide Fuel Cell stacks

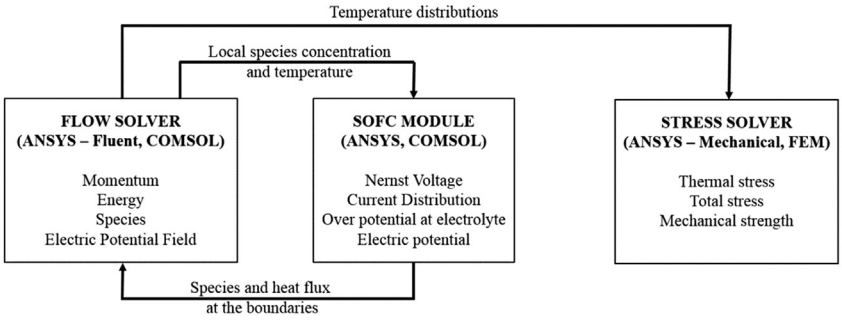

Fig. 1 – Coupling of a flow solver, a SOFC module and a stress solver [11].

Table 1 – The governing equations for mass, momentum and energy balance.

Continuity equation	$\nabla(\rho_{air}\overline{v}) = 0$	(1)
Momentum equation	$\nabla(\rho_{air}\overline{v}\overline{v}) = -\nabla p + \nabla\left[\mu_{air}(\nabla\overline{v} + (\nabla\overline{v}))^T\right]$	(2)
Energy equation	$\nabla\left(-\lambda\nabla T + \rho_{air}C_pT\cdot\overline{v}\right) = 0$	(3)

Where: ρ_{air} was the density of air, $\overline{v}$ was the velocity vector, μ_{air} was the air dynamic viscosity, p was the static pressure, C_p was the gas specific heat, λ was the thermal conductivity of the fluid.

were established using thermal-fluid models of fuel cell operation, while mechanical properties of stack elements were used in the modelling of thermal stresses. A coupled Computational Fluid Dynamics (CFD) and Computational Structural Mechanics (CSM) analysis was performed using the commercial software ANSYS Fluent and ANSYS Mechanical. An example of coupling a flow solver, a SOFC module and a stress solver is presented in Fig. 1 [11].

A full numerical model was based on the coupling of mass (1), momentum (2) and energy (3) balance equations with electrochemical reactions and electrochemical potential equations as well as the total strain (6) and stress–strain relationship (8) for materials and the model was described in details in a former paper [13].

The governing equations for mass, momentum and energy balance are summarized in Table 1.

Moreover, in the energy balance equation (4) for the k-th surface, emission, absorption and reflection of the thermal radiation by the solid boundary surface of the mSOFC stack and fuel cells tubes were taken into consideration [11,12]:

$$q_{out,k} = \varepsilon_k\sigma T_k^4 + (1-\varepsilon_k)q_{in,k} \tag{4}$$

where: $q_{out,k}$ was the energy flux leaving the k-th surface, ε_k was the surface emissivity, σ was the Boltzmann constant, T_k was the temperature at the k-th surface, $q_{in,k}$ was the energy flux incident to a surface from surroundings given as Eq. (5):

$$q_{in,k} = \sum_{j=1}^{N} F_{kj}q_{out,j} \tag{5}$$

where: F_{kj} was the dimensionless view factor.

The applied structural mechanics model assumed that fuel cell materials undergo linear thermoelastic deformation. The total strain based on the elastic, ε_{el}, and thermal, ε_{th}, components and was expressed as:

$$\{\varepsilon\} = \{\varepsilon_{el}\} + \{\varepsilon_{th}\} \tag{6}$$

Thermal strain vector was given as:

$$\{\varepsilon_{th}\} = \{\alpha \quad \alpha \quad \alpha \quad 0 \quad 0 \quad 0\}(T - T_{ref}) \tag{7}$$

where: α denoted the coefficient of thermal expansion (CTE), T was the temperature obtained from the thermos-fluid model during the first stage of the CFD simulation, T_{ref} was the stress free temperature.

The stress-strain, σ–ε, relationship for an isotropic, linear elastic solid material was given through the following relation:

$$\begin{Bmatrix}\sigma_{xx}\\ \sigma_{yy}\\ \sigma_{zz}\\ \sigma_{yz}\\ \sigma_{xz}\\ \sigma_{xy}\end{Bmatrix} = \frac{E}{(1+\nu)(1-2\nu)}\begin{bmatrix}1-\nu & \nu & \nu & 0 & 0 & 0\\ \nu & 1-\nu & \nu & 0 & 0 & 0\\ \nu & \nu & 1-\nu & 0 & 0 & 0\\ 0 & 0 & 0 & \frac{(1-2\nu)}{2} & 0 & 0\\ 0 & 0 & 0 & 0 & \frac{(1-2\nu)}{2} & 0\\ 0 & 0 & 0 & 0 & 0 & \frac{(1-2\nu)}{2}\end{bmatrix}\begin{Bmatrix}\varepsilon_{xx}\\ \varepsilon_{yy}\\ \varepsilon_{zz}\\ \varepsilon_{yz}\\ \varepsilon_{xz}\\ \varepsilon_{xy}\end{Bmatrix} - \frac{E\cdot\alpha\cdot\Delta T}{1-2\nu}\begin{Bmatrix}1\\1\\1\\0\\0\\0\end{Bmatrix} \tag{8}$$

where: E denoted the Young's modulus, ν was the Poisson's ratio of the model material, ε_{xx}, ε_{yy}, ε_{zz} were the normal strain values, whereas ε_{yz},ε_{xz},ε_{xy} were the shear strains in each plane.

The equivalent von Mises stress was calculated as:

$$\sigma_{vM} = \sqrt{\frac{1}{2}\cdot\left[\left(\sigma_{xx}-\sigma_{yy}\right)^2+\left(\sigma_{yy}-\sigma_{zz}\right)^2+\left(\sigma_{zz}-\sigma_{xx}\right)^2\right]+3\cdot\left(\sigma_{xy}^2+\sigma_{yz}^2+\sigma_{zx}^2\right)} \quad (9)$$

In the first step of the CFD calculations, the flow solver delivered local values of the velocity, pressure and temperature, which allowed visualization of the thermo-fluid conditions in the mSOFC stack. In parallel, thermo-electrochemical model available in the SOFC module for a single microtubular SOFC was solved to analyse the current density distribution and temperature distribution in the fuel cell. The heat flux obtained from the electrochemical model of a single mSOFC was implemented into the mSOFC stack to take into account electrochemically driven non-uniformities of the stack temperature. In the second step of the modelling, temperature distributions were forwarded to the stress solver. Based on the temperature distribution, stress distribution including the von Mises stress in ceramic material were estimated.

Geometry and numerical mesh of mSOFC stacks

The stack temperature predictions were based on a 48 anode-supported microtubular Solid Oxide Fuel Cell stack in two different configurations. In the first mSOFC design, fuel cells were distributed over four circular circumferences, with each of the four circles containing 12 fuel cells (Fig. 2a) denoted case C–I (circular-internal air inlet). In the second mSOFC configuration, a hexagonal fuel cells' distribution was assumed as shown in Fig. 2bc and defined as case H–E (hexagonal-external) with an external air cooling (Fig. 2b) or case H–I (hexagonal-internal) with an internal air cooling (Fig. 2c).

For both configurations of the mSOFC (Fig. 2a and b) fuel was introduced into the stack through the inlet manifold at the bottom part of the stack (empty holes in the red surfaces (in the web version)). A significant difference between analysed arrangements was in the method of supplying the cooling air. For the case C–I and case H–I, cold air entered the stack from air distributor located in the middle part of the stack and was radially distributed between fuel cells towards the mSOFC stack housing. For the case H–E with hexagonal fuel cells configuration cold air was supplied through the air collector with longitudinal slots located in the stack housing and flew towards the outlet air collector located in the centre of the stack. In addition to the mSOFC stack, both configurations contained also two manifolds, cylindrical or dodecagon housing, internal cylindrical or dodecagon collector of inlet/outlet air as well as internal and external support rings. The manifolds were located on both sides of the stack, one at the fuel inlet and other at the fuel outlet. The manifolds provided sealing for fuel flow through the mSOFC stack.

Meshes generated for the fluid-thermal model included 712 and 988 thousand tetrahedral computational cells for cases C and H, respectively, while that for the thermo-mechanical model consisted of 1.15 and 1.13 million of numerical cells, respectively.

Material properties

The thermal properties of the materials used for the study are given in Tables 2 and 3.

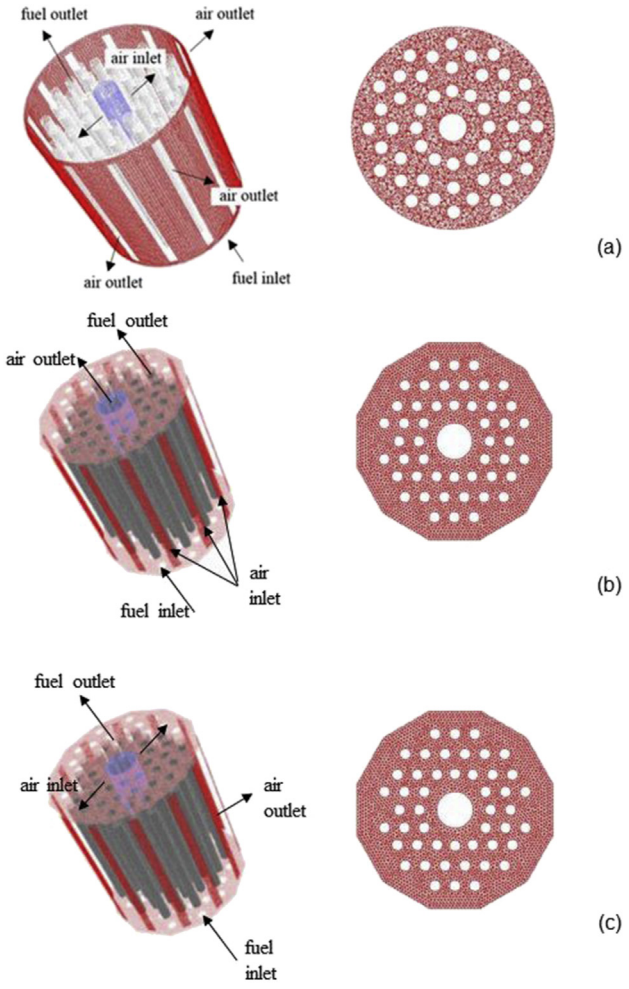

Fig. 2 – 48 anode-supported mSOFC stack, fuel cells distributed: (a) in four circular rows with an internal air flow direction (case C–I), (b) hexagonally with an external cooling air flow direction (case H–E), (c) hexagonally with an internal cooling air flow direction (case H–I).

Table 2 – Mechanical properties of mSOFC materials [10,14–19].

Property	mSOFC material		
	Anode (Ni-YSZ)	Electrolyte (YSZ)	Cathode (LSCF)
Coefficient of thermal expansion, CTE·10^{-6},1/K	12.2 [14]	10.3 [18]	13 [19]
Young's modulus, E, GPa	57 [14]	215 at 298 K 185 at 1073 K [17]	161 [19]
Poisson's ratio, ν [–]	0.28 [15]	0.32/0.313 [15]	0.32 [19]
Density, ρ, kg/m^3	4500 [16]	6050 [18]	6820 [19]
Thermal conductivity, λ, W/mK	1.83 [14]	2.2 [18]	1.31 [16]
Gas specific heat, C_p, J/kgK	500 [16]	600 [16]	470 [16]
Tensile yield strength, MPa	115 [17]	332/256 [15]	155 [10]
Compressive strength, MPa	100	1000 [17]	100 [17]
Stress free temperature, K	1473 [17]	1473 [17]	1323 [19]

Table 3 – Mechanical properties of mSOFC stack materials used in the FEM simulations [20–22].

Property	mSOFC material		
	Manifolds and seals macor machinable glass ceramic [20]	Housing & air distributor Hastelloy X [21]	Housing & air distributor Inconel X 750 [22]
Coefficient of thermal expansion, CTE·10^{-6} [1/K]	12.3	15.6	9.3
Young's modulus, E [GPa]	66.9[a]/40.5[b]	205/153[c]	213.7/127.5[c]
Poisson's ratio, ν [–]	0.29	0.32[a]	0.29
Density, ρ[kg/m^3]	2520	8220	8280
Thermal conductivity, λ[W/mK]	1.46[a]/1.25[b]	9.1/27.2[d]	12.0/23.65[c]
Gas specific heat, C_p [J/kgK]	790[a]	486/699[c]	431/716[c]
Ultimate tensile strength [MPa]	94[a]/41[b]	767/310[c]	758.4/241.3[c]
Tensile yield strength [MPa]	–	379/194[c]	320.6/189.6[c]
Compressive strength [MPa]	345 (to 900)	–	1175.5[e]

Description of symbols used in Table 3:
[a] At 25 [°C].
[b] At 800 [°C].
[c] Sheet at 25 [°C]/871 [°C].
[d] At 21 [°C]/816 [°C].
[e] At 704 [°C].

In order to simplify the computational effort the following assumptions were used in simulations: fuel cells' material properties were assumed for zero porosity, stress free temperature was equal to the consolidating temperature for each step of manufacturing process used for anodes and electrolytes and the operating temperature was equal to 750 °C.

Boundary conditions

Coupling of the thermo-fluid analysis with the thermo-mechanical method was used to evaluate the thermal stress distributions for two different mSOFC stack configurations and three different cases. First, temperature distributions were calculated and compared for considered cases. Then, the predicted temperature distributions were implemented into the thermo-mechanical model to estimate thermal stress distributions in the mSOFC stacks and to assess the effects of the geometry of flow channels as well as design of the inlet and outlet manifolds on the thermal elongations. To evaluate the fluid-thermal conditions of the mSOFC the CFD simulations were carried out using the ANSYS – Fluent 14.0 code with ANSYS Fuel Cell Tools module, while to estimate the thermo-mechanical behaviour of the mSOFC components the Finite Element Method (FEM) simulations were performed using the ANSYS Mechanical 15.0 code. Thus, the operating conditions of the all considered cases were as follows:

- for thermo-fluid model: the computational domain was the cathode air volume of the mSOFC stack; pure air was assumed as the working medium and it was treated as ideal gas, radiative heat transfer was taken into account via non-participating media by surface-to-surface model, local heat flux values along the electrochemically active surface of the mSOFC tubs were defined as 2425 W/m^2 and emissivity of 0.4, the inert part of the fuel cell tubes as well as the stack walls were defined as adiabatic,
- for thermo-mechanical model: structural constraints with one degree of freedom in the axial direction at the right outer surface of the stack housing was assumed, the reference temperature was equal to 25 °C, while supporting structure of the mSOFC stack had a constant temperature of 750 °C and this value of temperature along with the working temperature of fuel cells obtained in thermo-fluid model was implemented from the ANSYS – Fluent into the ANSYS Mechanical (Static Structural) software and used as

the load in the model. In addition, the following assumptions were made in the thermo-mechanical model: the stress free temperature value was assumed as the sintering temperature of the anode layer with the electrolyte and it was equal to 1473 K, while a connection of the anode and electrolyte layers with the cathode layer during the second sintering process was assumed at the sintering temperature of 1323 K. Moreover, material properties were assumed independent of porosity, the effect of gravity was neglected and the only load in the thermo-mechanical model was the working temperature of fuel cells estimated in the CFD modelling [13].

Simulations results

Computational Fluid Dynamics analyses provided the predicted temperature fields for each case. The CFD thermal fields were then implemented into the FEM model. Fig. 3 depicts examples of the temperature profiles in the MEA imported from the ANSYS Fluent to the ANSYS Mechanical module.

This step enabled to analyse the system behaviour in terms of thermo-fluid conditions and to determine the weak locations within the mSOFC system that are vulnerable as exposed to high stress.

The operational temperatures from CFD and initial FEM computing results are presented in Table 4 and they include basic data without the effect of the residual stress, which was also analysed graphically as contour maps of mechanical parameters in the considered mSOFC stack design cases. As expected, the case C–I was the worst case with the weakest cooling conditions as shown in Fig. 3a, while the case H–E with the external inlet air cooling has got the best cooling conditions. The temperature difference between fuel cells located close to the stack housing and those located near the axis of the stack was in the range 55–90 °C, however it should be mentioned that in the latter case H–E the size of the air inlet was bigger in comparison to the holes in the air distributor located in the middle of the stack at a constant value of the air inlet velocity. In consequence, the maximum axial, radial and total displacement of the assembly with supporting structure was the biggest for the circular mSOFC stack design (case C–I) and the smallest one for the hexagonal design with the external air cooling (case H–E). This stems from the quality of the cooling conditions and temperature values since higher temperatures cause greater deformation of the system. It is worth to notice that despite the significant temperature difference of 20 °C between the cases C–I and H–I, the difference in displacement between these cases was rather small.

The predictions of the radial displacement of the whole mSOFC stack system revealed that despite of the worst air cooling conditions for the case C–I the lowest value of the radial displacement was noticed for the fuel cells. The reason for such behaviour of the system can be its design as well as fuel cells distances from the middle of the system. However, a similar result was observed for both hexagonal configurations, i.e. cases H–E and H–I. Interesting is that the difference of the displacement are barely noticeable for the external fuel cells, while for them middle ones are significant. Table 4 shows that the lowest value of the von Mises stress of 538 [MPa] was noticed for the case C–I, while the biggest one for the case H–I and slightly smaller for the case H–E. It was quite surprising taking into account that the fuel cells of case C–I had highest temperatures. However, it could be explained by the fact, that the cases H–E and H–I based on dodecagon

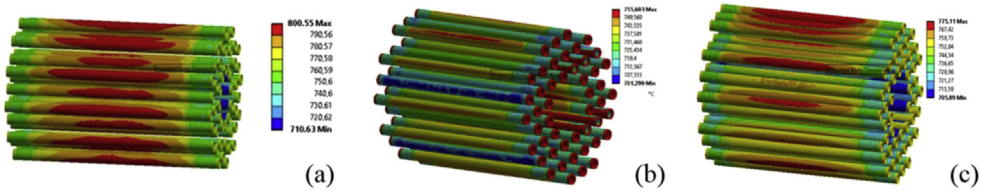

Fig. 3 – Thermal distribution in the MEA imported to the ANSYS Mechanical module: (a) case C–I, (b) case H–E, (c) case H–I.

Table 4 – A summary of key findings for three considered cases of the mSOFC stack design with supporting structure.

Feature	Case C–I (cylindrical, internal inlet air cooling)	Case H–E (hexagonal, external inlet air cooling)	Case H–I (hexagonal, internal inlet air cooling)
Min. temperature of fuel cell operation [°C]	710.63	701.3	705.89
Max. temperature of fuel cell operation [°C]	800.55	755.6	775.11
Max. axial displacement [mm]	1.34	1.24	1.244
Max. radial displacement [mm]	0.496	0.487	0.488
Max. total displacement [mm]	1.345	1.269	1.277
Min. radial displacement in system [mm]	−0.331	−0.356	−0.357
Max. radial displacement in system [mm]	0.382	0.409	0.408
Max. compressive axial stress [MPa][a]	−503.76	−478.08	−480.71
Max. tensile axial stress [MPa]	544.16	687.16	698.66
Von Mises stress [MPa][a]	538.42	746.74	756.26

[a] Without residual stress.

Table 5 – Comparison of the axial stress and the total axial stress values at chosen cross-sections for different mSOFC stack design configurations sections without supporting structure.

Case	Cross section I top side of external fuel cell				Cross section II bottom side of internal fuel cell			
	Z [mm]	Anode	Electrolyte	Cathode	Z [mm]	Anode	Electrolyte	Cathode
	Axial stress values at the operating conditions [MPa]							
Case C–I	61	7.52	428.73	−139.12	61	2.81	410.82	−115.11
Case H–E	61	3.49	409.55	−111.41	61	4.92	415.91	−123.63
Case H–I	61	6.71	425.50	−126.09	61	1.84	407.78	−113.39
	Total axial stress values (operating conditions & residual) [MPa]							
Case C–I	61	2.59	−283.99	34.66	61	−2.11	−301.90	58.67
Case H–E	61	−1.43	−303.17	62.37	61	−0.002	−296.81	50.15
Case H–I	61	1.78	−287.22	47.69	61	−3.11	−304.94	60.39

Table 6 – Comparison of axial stress and total axial stress values at chosen cross sections for different mSOFC stack design configurations with supporting structure.

Case	Cross section I top side of external fuel cell				Cross section II bottom side of internal fuel cell				Cross section III bottom side of middle fuel cell			
	Z [mm]	Anode	Electrolyte	cathode	Z [mm]	Anode	Electrolyte	cathode	Z [mm]	Anode	Electrolyte	Cathode
	Axial stress values at the operating conditions [MPa]											
Case C–I	61	−77.1	129.8	−386.2	61	12.1	447.8	−84.5	61	−15.2	351.9	−192.9
Case H–E	61	−50.6	218.6	−266.5	61	−40.4	255.4	−254.9	61	−34.7	278.1	−236.5
Case H–I	61	−68.8	157.9	−346.0	61	−25.2	313.8	−189.5	61	−25.3	314.0	−198.4
	Total axial stress values (operating conditions & residual) [MPa]											
Case C–I	61	−82.0	−582.9	−212.4	61	7.2	−264.9	89.3	61	−20.2	−360.7	−19.1
Case H–E	61	−55.5	−494.1	−92.7	61	−45.3	−457.3	−81.2	61	−39.7	−434.6	−62.7
Case H–I	61	−73.7	−554.8	−172.2	61	−30.2	−398.9	−15.7	61	−30.2	−398.7	−24.61

housing, which accumulates corner stresses. Thus, the conclusion was that structures with angular corners are less practical and exposed to higher stresses. Moreover, the compressive axial stresses are the highest again for the case C–I and the lowest for the case H–E. However the difference between cases H–E and H–I, both dodecagon housing with hexagonal fuel cell distributions, with external or internal inlet air cooling was barely noticeable. One of the important features the FEM model provides is the tensile axial stress magnitude, which was the highest for the case H–I and the lowest for the case C–I. The difference was quite significant for the case H–I of around 150 [MPa] in respect to the case C–I. This enables to conclude that the relationship between the mean working temperature and tensile axial stress was weaker than the impact of the geometrical model and corner constructions onto the tensile axial stress. Moreover, the predicted values of the tensile axial stress for cases H–E and H–I were similar.

Tables 5 and 6 present comparison of the axial stress and the total axial stress values for different mSOFC stack design configurations with 48 anode supported fuel cells without and with supporting structure, respectively. The axial stresses and the total axial stresses in the stack were analysed along the mid-thickness lines, respectively of the anode, electrolyte and cathode at the position of Z = 61 [mm] and for two cell types: an external fuel cell ("cross-section I") as well as for an internal fuel cell marked "cross-section II". In addition, results for external, middle and internal fuel cells were presented in Table 6 for top and bottom side, respectively. These cross-sections are labelled in Fig. 4 at the right side.

The cross-section I was subjected to the weakest cooling conditions in the stack for cases C–I and H–I, while to the

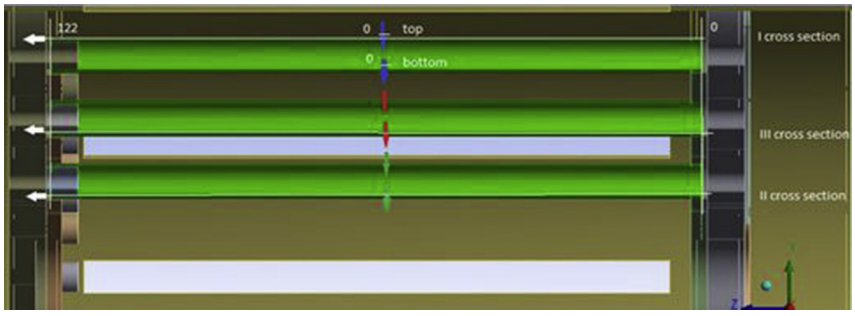

Fig. 4 – Selected half cross-section regions of the mSOFC stack geometry. The length distance is measured from the point marked "0" in the direction of white arrows.

strongest cooling conditions the case H–I was exposed. In contrast, the cross-section II of fuel cells located close to the axis of the stack experienced the strongest cooling for cases C–I and H–I and weakest cooling effects for case H–E.

In this study, only the axial component of the stresses in fuel cells will be presented in details due to lower magnitude of the radial stress component.

It follows from Table 5 that a FEM analysis for the mSOFC stack design configurations without supporting structure revealed the effects of high and spatially variable operating temperature and different CTE of individual fuel cell layers on the state of stress. At the top side of the external fuel cell (for cross-section I) the axial stresses at the operating conditions with the residual stress are the highest for the case C–I and the lowest for the case H–E, while at the bottom side of internal fuel cell the highest stresses are for the case H–E, the lowest for the case H–I. However, comparing the total axial stresses, which include the residual stress, the opposite relationship can be observed. The most preferably appears then the case C–I.

It results from the detailed FEM analysis of axial stresses and total axial stresses, for different mSOFC stack design configurations with supporting structure presented in Table 6, that a significant impact of the supporting structure joined with the mSOFC stack by ceramic sealants was simulated.

Noticeable is also an unusual relationship of axial stress values at the operating conditions for the chosen cross sections. Interesting is that the location of fuel cell (top or bottom) has an impact on stress within the fuel cell layers. If the stress was the highest, for the selected fuel cell layer in three cases at the top part of the fuel cell, then for the same layer at the bottom part of the fuel cell and the same case the stress was the smallest one and vice versa. It should be noticed that extreme stresses occurred only for cases C–I and H–E, while for the case H–I they were always intermediate. Moreover, when the greatest stress for chosen layer and side of the fuel cell was noted for the case C–I, then for the case H–E the lowest value was found there and vice versa. An important outcome is also that if the axial stress was the highest for the cathode, then it was also the highest in the anode, while in the

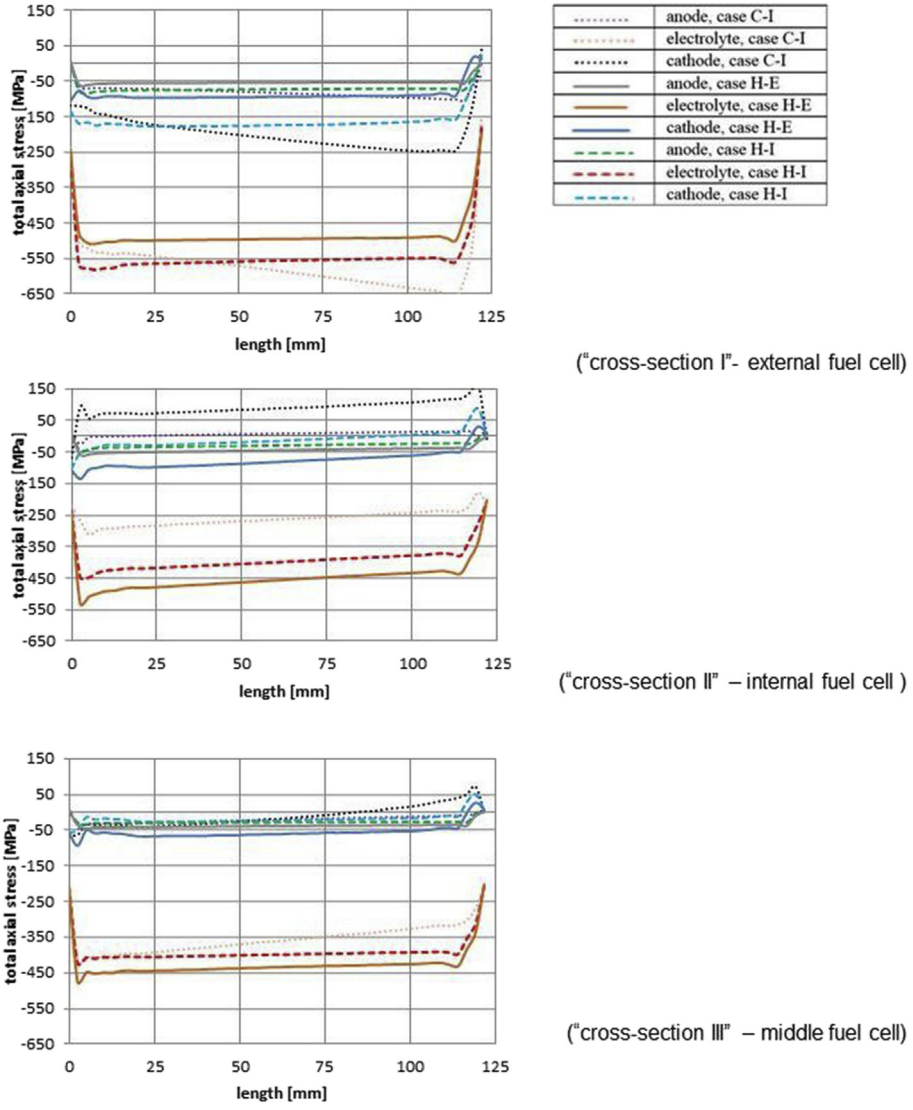

Fig. 5 – Total axial stress distribution in the assembly: mSOFC stack (configurations: case C–I, H–E and H–I), sealants, manifolds and housing along horizontal centrelines of each layer for cross-sections I–III.

electrolyte was the smallest for a chosen fuel cell cross section. Similarly, as the electrolyte axial stresses are the greatest in the present study, then at same cross-section the smallest axial stress values are found in the cathode and anode.

The total axial stress at the operating conditions that included residual stress at the top side of the external fuel cell indicated the highest absolute value for the case C–I as the most harmful, with its lowest values for the case H–E. However, at the bottom side of the middle and internal fuel cells (cross sections II and III) the total axial stresses are greatest for the case H–E and smallest for the case C–I with an exception for the cathode at the cross section II, where the total axial stresses are greatest for the case C–I (only stretching/displacement) and lowest for the case H–I.

Comparing the three computational cases indicates the smallest axial stresses with residual component at the top side of the fuel cell for the case H–E with hexagonal fuel cells configuration and the external cold air inflow, while for the bottom side of the fuel cells it was the case C–I configuration with four circular fuel cell rows and internal cold air inflow, with the exception discussed above.

Fig. 5–6 present visually the obtained profiles of the total axial stress in the assembly containing the cylindrical (case C–I) or dodecagon (cases H–E and H–I) mSOFC stack designs, sealants, manifolds and housing. They are for air cooling flow from the external side to the middle part of the stack (case H–E) and from the internal side towards the outer part of the mSOFC stack housing (cases C–I, H–I) along horizontal centrelines of each layer for cross-sections I–III.

The FEM predictions reveal strong heterogeneity of the axial stress along the length of the fuel cell stack for the analyses including the supporting structure. Tensile (positive) stresses were for the fuel inlet side, then they shifted toward negative compressive stresses at the air inlet side, which results from the interaction of the supporting structure with the fuel cells through sealants, assuming structural constraints with one degree of freedom used in the axial direction at the right outer surface of the stack housing from the air inlet side. Therefore, the whole system moves toward the fuel inlet, so fuel cells on that side are more stretched. Due to considerable radial dimensions of the mSOFC stack, it increases perceptibly in that direction and it has a major role in radial deformation

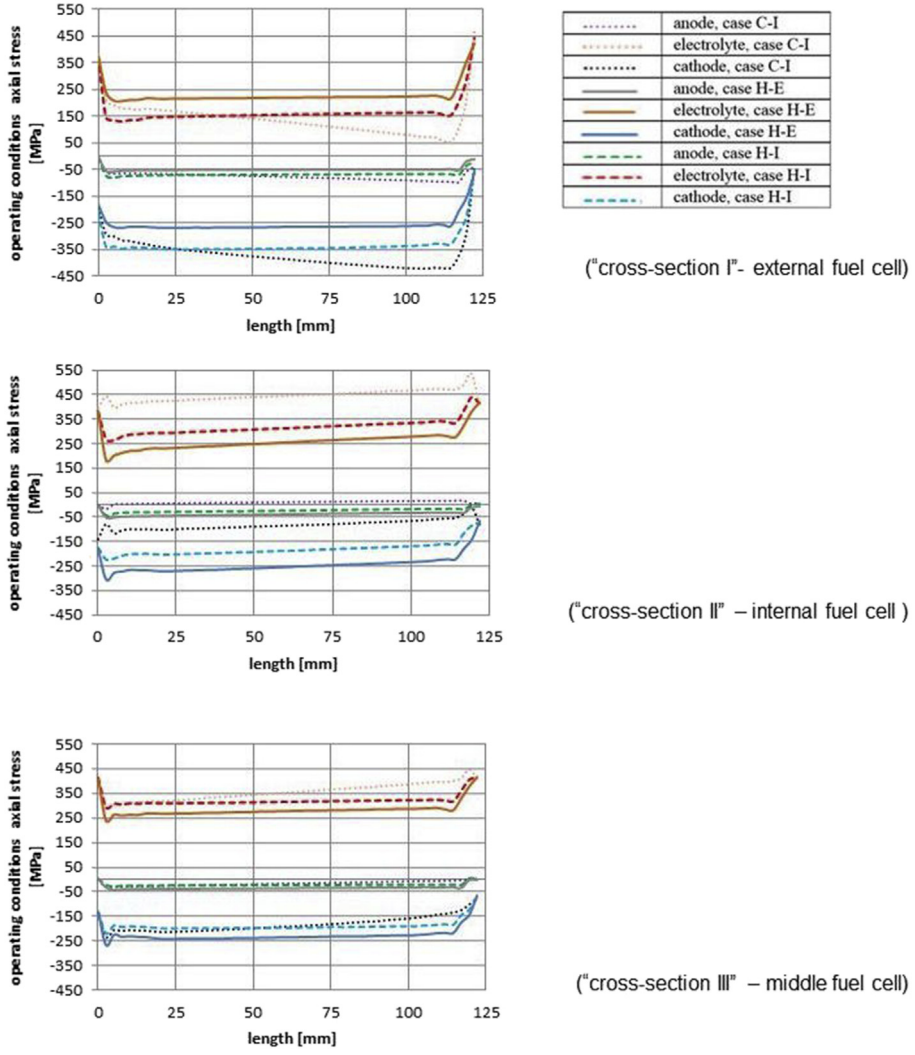

Fig. 6 – Axial stress distribution as a function of the operating temperature in the assembly: mSOFC stack (configurations: cases C–I, H–E and H–I), sealants, manifolds and housing along horizontal centrelines of each layer for cross-sections I–III.

with a stronger shape change of the outer row of fuel cells than of that for the internal row. Significant impact of the supporting structure onto the operating fuel cell conditions induces higher values of stresses.

Evaluation of the effects of the external or internal air cooling inflow side for the mSOFC stack design configurations with the supporting structure has not shown a significant influence on the behaviour of stresses, but the following tendencies were noticed:

- the axial stresses are more compressive for the outer row of fuel cells are bigger in comparison to those for the internal row of fuel cells for the analyses without consideration of the residual stress,
- when the residual stress was taken into account, higher absolute value and more compressive axial stress on the side of the outer row of fuel cells were noticed,
- the trend is also observed for the middle row of fuel cells (with one exception for the case H–E) when the cold air was introduced from the external side of the housing and the total axial stresses for the middle fuel cells were the smallest and the least compressive stress was calculated in comparison to internal and external fuel cells,
- for the middle row of fuel cells the axial compressive stress without the residual component was the minimum, while the tensile stress was the maximum.

The thermal stress depends in large measure on the CTE mismatches between different materials and is a subject of temperature gradients. Therefore, the total axial compressive stresses for all layers and fuel cell rows were lower on that side of the fuel cells (top/bottom), where the cold air inlet (external/internal) was assumed, with one exception of case H–E: for the anode and electrolyte of the fuel cells located at the outside part. However, as expected in all considered cases, the total axial stresses appeared in the electrolyte layer (compressive stress) and their smallest values were estimated in the anode (both tensile and compressive stresses). Moreover, when comparing the case H–E with the case H–I (the same hexagonal fuel cells configuration), the case H–E was characterized by less axial compressive stress for the top side of the fuel cell at the cross section I and more compressive stress for the bottom side at the cross sections II and III. It was valid for all fuel cell layers in both FEM analyses of the mSOFC stack and with or without the supporting structure as it was shown in Figs. 5–6.

In terms of strength features the performed analyses showed the following:

- Macor ceramic collectors should not be damaged in any of considered cases,
- in the Inconel X 750 housing the regions such as corners of the external stack housing, and contact points with air distributor need special attention for cases H–E and H–I as well as for the contact regions between housing and air distributor of Hastelloy X and manifolds for the case C–I, due to large cut-outs in the material,
- neither the anode nor the electrolyte should be affected by the thermomechanically induced stress in any cases under examination,
- the only reservations can be addressed to the cathodes, which are subjected to large predicted axial stresses for the external row of fuel cells, but only for the top side in the cross section I and the case H–I as well as for two positions at the top and bottom for the external fuel cells in the case C–I. In particular, the risk of the cracks could appear in the cathode for the bottom side of the external fuel cells and the top side of the middle fuel cells for the case H–I and for both positions of the external fuel cells for the case H–E,
- another important point is that in the analyses of the mSOFC stack designs without the supporting structure and including the residual stress, none of fuel cell layer for all considered cases became too highly stressed, which means the mSOFC stacks were not exposed to damage according to the deterministic model.

The predictions reveal that the housing of Inconel X 750 in contact with the ceramic manifolds may produce compressive stresses in the manifolds, which have higher value of the CTE than Inconel. Due to heating, manifolds will tend to extend more than the housing, while in the housing the tensile stress in the contact regions will increase. On the other hand, if the Hastelloy X material will be used for housing, an opposite behaviour can be observed. The tensile stress will increase in the manifolds in the contact regions, while the compressive stress will appear in the housing. Therefore, to avoid cracks in the system close CTE materials are recommended.

Conclusions

In the present work temperature profiles generated in the CFD simulations by a thermal-fluid model were applied to calculate thermal stress distributions in the mSOFC stacks. The resulted maximum total axial stresses and the effects of temperature obtained for both the circular and hexagonal stack designs were compared. The FEM results enable visualisation of the thermomechanically induced stress distributions. Obtained results also helped assess the effects of the geometry of flow channels, interconnectors, manifolds as well as designs with the inlet and outlet manifolds. The maximum axial and radial thermal elongations during free mechanical load of the stacks were estimated for both stack designs. Despite careful analyses, it is yet difficult to state clearly, which of the considered mSOFC stack design configurations is the optimal solution. The comparison indicates the case H–E as the best solution from the thermal stress point of view, which was the only case of the external inlet cold air flow. However, it should be mentioned that location of cold air flow inlet plays an important role. For all considered cases a constant flow velocity was assumed, thus a simple relationship was obtained: the bigger the air inlet surface, the better cooling. The largest air inlet surfaces were assumed for the case H–E and the smallest one for the case C–I, which may influence the final assessment of the thermomechanical mSOFC system behaviour. Nevertheless, it was shown that the thermal stress results indicated possibility of improving shape of the housing in the case H–E and H–I, where the dodecagon housing was assumed. Larger total axial stresses in the corners may lead to cracks and therefore should be limited to

avoid stress concentration in the corners. To reduce the stress accumulation and to achieve higher reliability of the mSOFC system the use of circular cross-section of the housing is recommended.

The presented CFD and FEM results showed that modelling can help to understand heat transfer conditions in the microtubular Solid Oxide Fuel Cell stack and accurately predicting temperatures within the stack. Precise modelling of the thermal and mechanical conditions is one of the main challenges in improving its thermal management and decreasing fuel cell degradation due to thermal stress induced by uneven temperature distributions.

Acknowledgement

The research programme leading to these results received funding from the European Union's Seventh Framework Programme (FP7/2007-2013) for the Fuel Cells and Hydrogen Joint Technology Initiative under grant agreement no [278629]. Information contained in the paper reflects only view of the authors. The FCH JU and the Union are not liable for any use that may be made of the information contained therein.

Acknowledgments are due to the partners of SUAV: E. de Wit, R. Makkus, J. P. Brouwer of HyGear Fuel Cell Systems B.V., The Netherlands; M. Kendall, K. Kendall of Adelan Ltd., UK; T. Hargitai, F. Silversand, A. K. Jannasch, M. Lenberg, Ch. Karlsson of Catator AB, Sweden; V. Antonucci, A.S. Arico, M. Ferraro of Consiglio Nazionale delle Ricerche, Italy; G. Schramm of EADS Deutschland GmbH, Germany; J. Price, T. Owen, M. Maynard of EADS UK Ltd.; E. Erdle of efceco, Germany; R. Steinberger - Wilckens, A. Dhir, B. Hari, T. Meadowcroft of The University of Birmingham, UK; E. Georges, J. Chapuis, J. M. Masenelli of Survey Copter, France.

The work was also financed from the Polish research Funds awarded for the project No. W20317.PR/2011 of international cooperation within SUAV in years 2011–2014.

REFERENCES

[1] Liso V, Olesen A Ch, Nielsen MP, Kaer SK. Performance comparison between partial oxidation and methane steam reforming processes for solid oxide fuel cell (SOFC) micro combined heat and power (CHP) system. Energy 2011;36:4216–26. http://dx.doi.org/10.1016/j.energy.2011.04.022.

[2] Mounir H, Belaiche M, El Marjani A, El Gharad A. Thermal stress and probability of survival investigation in a multi-bundle integrated planar solid oxide fuel cells IP-SOFC (integrated planar solid oxide fuel cell). Energy 2014;66:378–86. http://dx.doi.org/10.1016/j.energy.2014.01.017.

[3] Vijay P, Hosseini S, Tade MO. A novel concept for improved thermal management of the planar SOFC. Chem Eng Res Des 2013;91:560–72. http://dx.doi.org/10.1016/j.cherd.2012.09.004.

[4] Fardadi M, Mueller F, Jabbari F. Feedback control of solid oxide fuel cell spatial temperature variation. J Power Sources 2010;195(13):4222–33. http://dx.doi.org/10.1016/j.cherd.2012.09.004.

[5] Grondin D, Deseure J, Zahid M, Garcia MJ, Bultel Y. Optimization of SOFC interconnect design using multiphysic computation. In: 18th European Symposium on Computer Aided Process Engineering – ESCAPE18, 841–846; 2008.

[6] Peksen M. A coupled 3D thermofluid-thermomechanical analysis of a planar type production scale SOFC stack. Int J Hydrogen Energy 2011;36:11914–28. http://dx.doi.org/10.1016/j.ijhydene.2011.06.045.

[7] Peksen M, Al-Masri A, Blum L, Stolten D. 3D transient thermomechanical behaviour of a full scale SOFC short stack. Int J Hydrogen Energy 2013;38:4099–107. http://dx.doi.org/10.1016/j.ijhydene.2013.01.072.

[8] Nakajo A, Mueller F, Brouwer J, Van herle J, Favrat D. Mechanical reliability and durability of SOFC stacks. Part II: modelling of mechanical failures during ageing and cycling. Int J Hydrogen Energy 2012;37:9269–86. http://dx.doi.org/10.1016/j.ijhydene.2012.03.023.

[9] Boigues-Munoz C, Santori G, McPhail S, Polonara F. Thermochemical model and experimental validation of a tubular SOFC cell comprised in a 1 kW_{el} stack designed for μCHP applications. J Hydrogen Energy 2014;39:21714–23. http://dx.doi.org/10.1016/j.ijhydene.2014.09.021.

[10] Delette G, Laurencin J, UsseglioViretta F, Villanova J, Bleuet P, Lay-Grindler E, et al. Thermo-elastic properties of SOFC/SOEC electrode materials determined from three-dimensional microstructural reconstructions. Int J Hydrogen Energy 2013;38:12379–91. http://dx.doi.org/10.1016/j.ijhydene.2013.07.027.

[11] Wei SS, Wang TH, Wu JD. Numerical modeling of interconnect flow channel design and thermal stress analysis of a planar anode-supported solid oxide fuel cell stack. Energy 2014;69:553–61. http://dx.doi.org/10.1016/j.energy.2014.03.052.

[12] Peksen M. 3D transient multiphysics modelling of a complete high temperature fuel cell system using coupled CFD and FEM. Int J Hydrogen Energy 2014;39:5137–47. http://dx.doi.org/10.1016/j.ijhydene.2014.01.063.

[13] Pianko-Oprych P, Zinko T, Jaworski Z. Modeling of thermal stresses in a microtubular Solid Oxide Fuel Cell stack. Journal of Power Sources [submitted to the Journal on 2nd of November 2014].

[14] Cui D, Cheng M. Numerical analysis of thermal and electrochemical phenomena for anode supported microtubular SOFC. AIChE J 2009;55:771–81. http://dx.doi.org/10.1002/aic.11697.

[15] Nakajo A, Stiller C, Harkegard G, Bolland O. Modeling of thermal stresses and probability of survival of tubular SOFC. J Power Sources 2006;158(1):287–94. http://dx.doi.org/10.1016/j.jpowsour.2005.09.004.

[16] SUAV data, internal project report. 2014.

[17] Li J, Lin Z. Effects of electrode composition on the electrochemical performance and mechanical property of micro-tubular solid oxide fuel cell. Int J Hydrogen Energy 2012;37:12925–40. http://dx.doi.org/10.1016/j.ijhzdene.2012.05.075.

[18] Anderman Industrial Ceramics Ltd. Zirconia Yttria Stabilised, brochure. 2014.

[19] Serincan MF, Pasaogullari U, Sammes NM. Thermal stresses in an operating micro-tubular solid oxide fuel cell. J Power Sources 2010;195:4905–14. http://dx.doi.org/10.1016/j.jpowsour.2009.12.108.

[20] Corning MACOR machinable glass ceramic 01, 02, brochure. 2014.

[21] Haynes International Hastelloy X Alloy, brochure. 2014.

[22] Inconel special metals alloy X 750, brochure. 2014.

Symbols

C_p: gas specific heat, J/kgK
E: Young's modulus, GPa
F_{kj}: dimensionless view factor, –
$q_{in,k}$: energy flux, W/m^2
$q_{out,k}$: energy flux leaving the k-th surfaces, W/m^2
p: pressure, Pa
T: temperature, K
T_k: temperature at the k-th surface, K
T_{ref}: stress free temperature, K
x,y,z: Cartesian coordinates, m
α: coefficient of thermal expansion, 10^{-6}/K
ε: total strain, –
ε_{el}: elastic strain, –
ε_k: surface emissivity
ε_{th}: thermal strain, –
λ: thermal conductivity, W/mK
μ_{air}: air dynamic viscosity, Pas
ν: Poisson's ratio, –
ρ: density, kg/m^3
ρ_{air}: density of air, kg/m^3
σ: stress, MPa
CFD: computational fluid dynamics
CTE: coefficient of thermal expansion
CSM: computational Structural Mechanics
FEM: finite element method
SOFC: Solid Oxide Fuel Cell